DESIGN AND EXPERIMENTAL STUDY OF A BIONIC ROTARY BLADE

Qing JIANG, Liangyuan XU, Hui QI, Weiqiang NI
School of Engineering, Anhui Agricultural University, Hefei 230036, China
E-mail: jtao@ahau.edu.cn

***ABSTRACT**: Rotary tillage operation is one of the core technologies in the agricultural mechanization. The effectiveness, efficiency and energy consumption of rotary tillage operation directly determine the application and popularization of agricultural machinery and equipment technologies in China. Currently, the commonly used rotary blades are energy-consuming but give poor performance, so it is very necessary to further develop cutting tools with less energy consumption and better performance. This paper extracts profile curves from the main tooth form of the moving chela of river crab, optimizes its structure and selects the curve that is most applicable to the tooth profile machining of rotary blades. Through the numerical simulation analysis, this paper performs stress and deformation analysis on the working conditions of different scoop surfaces of the prototype rotary blade and the bionic rotary blade, respectively. The stress and deformation of the bionic rotary blade improve greatly during the operation, which increases the structural stability and service life of the cutting tool. Through soil statics analysis, it is found that the bionic rotary blade hardly extrudes soil when working. This paper also carries out a comparison test on the field operation performance. Judged by the operating indicators, the performance of the bionic rotary blade is much better. This design of bionic rotary blade is of great research and practical value to reducing its energy consumption and improving its operation performance.*

***KEYWORDS**: agricultural machinery, bionic, rotary blade, numerical simulation analysis, operation performance.*

1 INTRODUCTION

The main functional component of a rotary cultivator is the rotary blade. The design and choices of the rotary blade structure and shape directly affects the performance and energy consumption of the tool. The rotary cutting tools commonly used in China include chisel-shaped blades, rectangular blades and bent blades. In light of the problems in the operation of rotary blades, it is necessary to conduct experimental study on the rotary tillage mechanism and performance so as to optimize the design of rotary blades. Now researchers are focusing on mitigating or eliminating the current drawbacks of rotary blades by optimizing the rotary blade structure, blade shape and surface friction characteristics so as to improve the quality of soil work (Lu et al., 2015; Gill and Vanden Berg, 1967; Zeng, 1995; Ren et al., 1999).

By taking the chelipeds of the river crab as the bionic object, this paper develops a kind of bionic rotary blade, and provides rigorous scientific proof based on relevant theories and by software analysis. Through field test, this paper compares the performance of the prototype rotary blade and the bionic rotary blade.

2 DESIGN OF THE BIONIC ROTARY CUTTING TOOL

2.1 Structural analysis of the crab cheliped

Crabs mainly use their chelipeds to cut and break the soil. A cheliped consists of a moving chela and a stationary chela, as shown in Figure 1a and 1b. The moving and stationary chelae contain a number of teeth arranged in tooth form and can be well engaged.

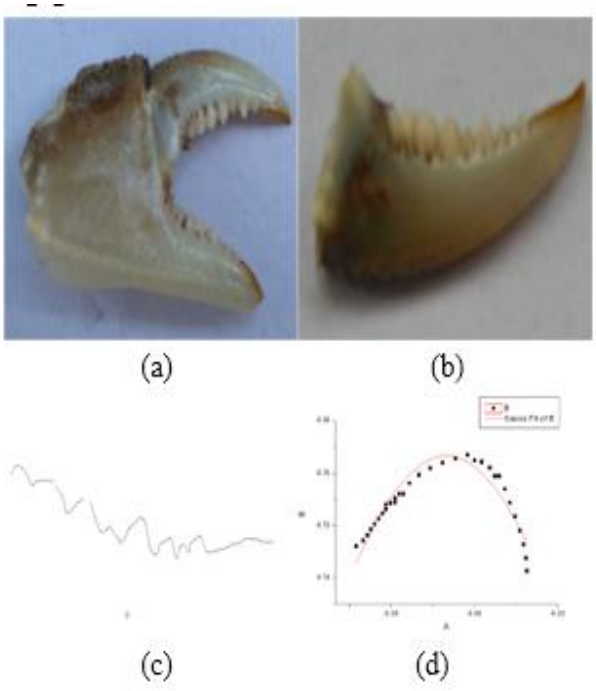

Figure 1. Structural analysis diagrams of the cheliped (a. Structure of the cheliped; b. Structure of the moving chela; c. Vector diagram of the tooth profile curve of the moving chela; d. tooth profile curve analysis of the cheliped**)**

2.2 Extraction and fitting of the tooth profile curves of the crab cheliped

The tooth profile curve vector diagram extracted through software analysis was enlarged, as shown in Figure 1c. On the moving chela of the crab cheliped, each single tooth form consists of a round top and a convex curve on each side, and there are smooth transitions between teeth, which can alleviate the stress concentration, increase the mechanical strength of the crab cheliped and reduce the soil-to-cheliped wear. At the same time, while the sharp angle of the cheliceral tooth is maximised, the top curve should be as smooth as possible to improve the stress conditions of the cheliceral teeth in the soil and reduce soil adhesion (Ding and Peng, 1995; Tong et al., 1994; Ren et al., 1999). The convex curves on the two sides can reduce the cutting resistance, which helps tear the soil apart and cut off the crop roots. With the help of Geomagic studio and through the curve fitting by Orgin8 (Tong et al., 1998; Gill et al., 1967; Luo 2005), the equation of the sawtooth curve on the moving chela can be expressed as Equation (1).

$$y=(0.03766/(0.11282*\mathrm{sqrt}(PI/2)))*\exp(-2*((x+0.07006)/0.11282)^2) \quad (1)$$

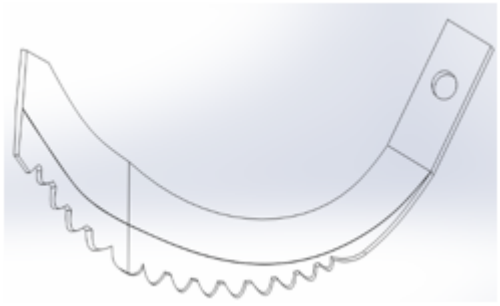

Figure 2. Schematic diagram of the bionic rotary cutting tool

2.3 Sawtooth design of the bionic rotary cutting tool

As shown in Figure 1d, the tooth tip angle directly affected the strength and sharpness of the tooth edge. Therefore, the tooth tip angle should be large. In order to reduce the resistance in rotary tillage and achieve good quality of soil cutting and roots and stems crushing, the tooth throat angle should also be large. Figure 2 schematic diagram of the bionic rotary cutting tool shows the best tooth characteristics for soil cutting and breaking.

The physical specimen of the bionic rotary blade designed and produced according to the tooth form in Equation (1) is shown in Figure 3a. The physical specimen of the prototype rotary blade is shown in Figure 3b:

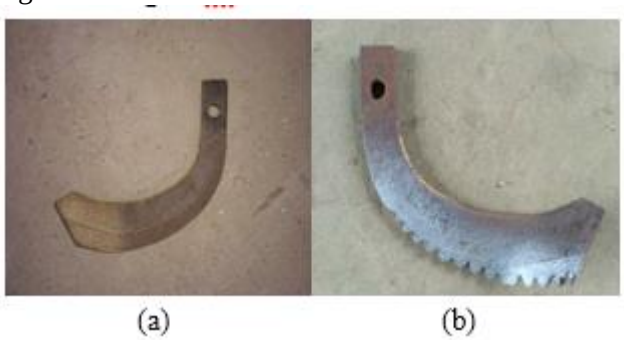

Figure 3. Pictures of the prototype and bionic rotary blades (a. Picture of the rotary cutting tool; b. Picture of the prototype rotary cutting tool**)**

3 NUMERICAL SIMULATION ANALYSIS OF THE ROTARY CUTTING TOOLS

3.1 Statics analysis and comparison of the rotary cutting tools

3.1.1 Statics analysis of the prototype rotary cutting tool

The prototype rotary blade had complex surfaces, so they were divided into small tetrahedral meshes in order to obtain more accurate data

parameters (Zhu et al., 2014; Ge et al., 2007). When the rotary blade was working, the parts that touched the soil were successively the side edge, the transition edge, the entire edge and the sidelong edge. Therefore, the boundary condition for the application of force was to apply a force of 500N vertically to the blade on the side edge, sidelong edge and full edge (Qu, 1987; Duan et al., 2005), and then analysis could be performed according to the total deformation and stress results.

The average pressure loaded on the side edge alone is expressed in (2);

$$P = \frac{F}{S} = \frac{500N}{826.54mm^2} = 0.6Mpa \quad (2)$$

The average pressure loaded on the sidelong edge alone is expressed in (3);

$$P = \frac{F}{S} = \frac{500N}{418.18mm^2} = 1.19Mpa \quad (3)$$

The average pressure loaded on the full edge is expressed in (4);

$$P = \frac{F}{S} = \frac{500N}{1244.72mm^2} = 0.4Mpa \quad (4)$$

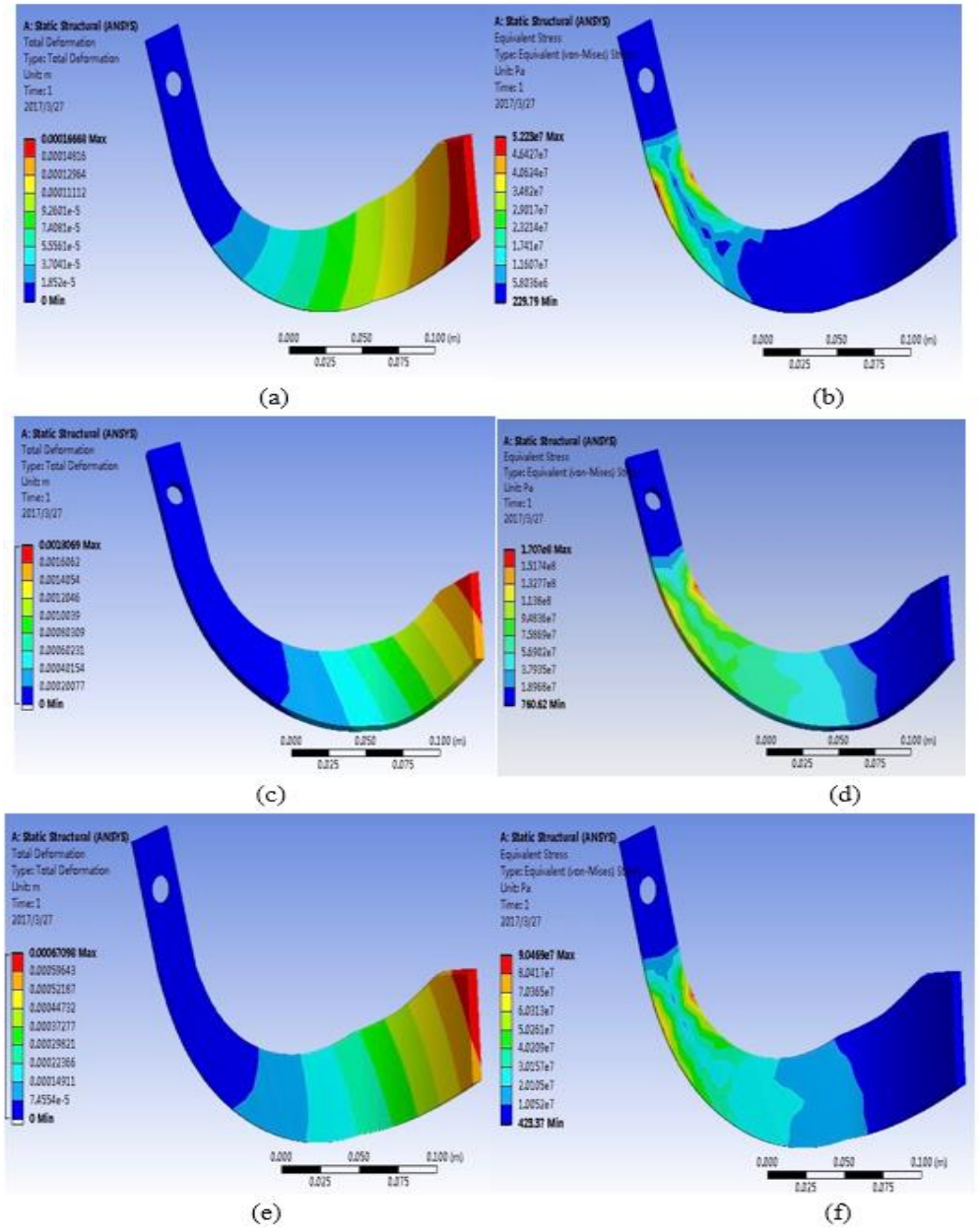

Figure 4. Force analysis diagrams of the prototype rotary blade (a. Total deformation of the loaded prototype rotary blade side edge; b. Total stress of the loaded prototype rotary blade side edge; c. Total deformation of the loadedprototype rotary blade sidelong edge; d. Total stress of the loaded prototype rotary blade sidelong edge; e. Total deformation of the loaded prototype rotary blade full edge; f. Total stress of the loaded prototype rotary blade full edge**)**

As can be seen from Fig.4a and Fig.4b, when load was applied to the side edge, the maximum deformation was 0.167mm, which occurred on the tip of the sidelong edge, and then decreased towards the side edge. The minimum deformation occurred at the handle. The maximum stress was 52.23Mpa, which occurred on the inner and outer sides of the joint between the handle and the tool face, and then extended outward and decreased gradually.

As can be seen from Fig.4c and Fig.4d, when load was applied to the sidelong edge, the maximum deformation was 1.807mm, which occurred on the tool tip after the sidelong edge, and then decreased towards the side edge. The minimum deformation occurred at the handle and part of the side edge. The maximum stress was 17.07Mpa, which occurred on the inner and outer sides of the joint between the handle and the tool face, and then extended outward and decreased gradually.

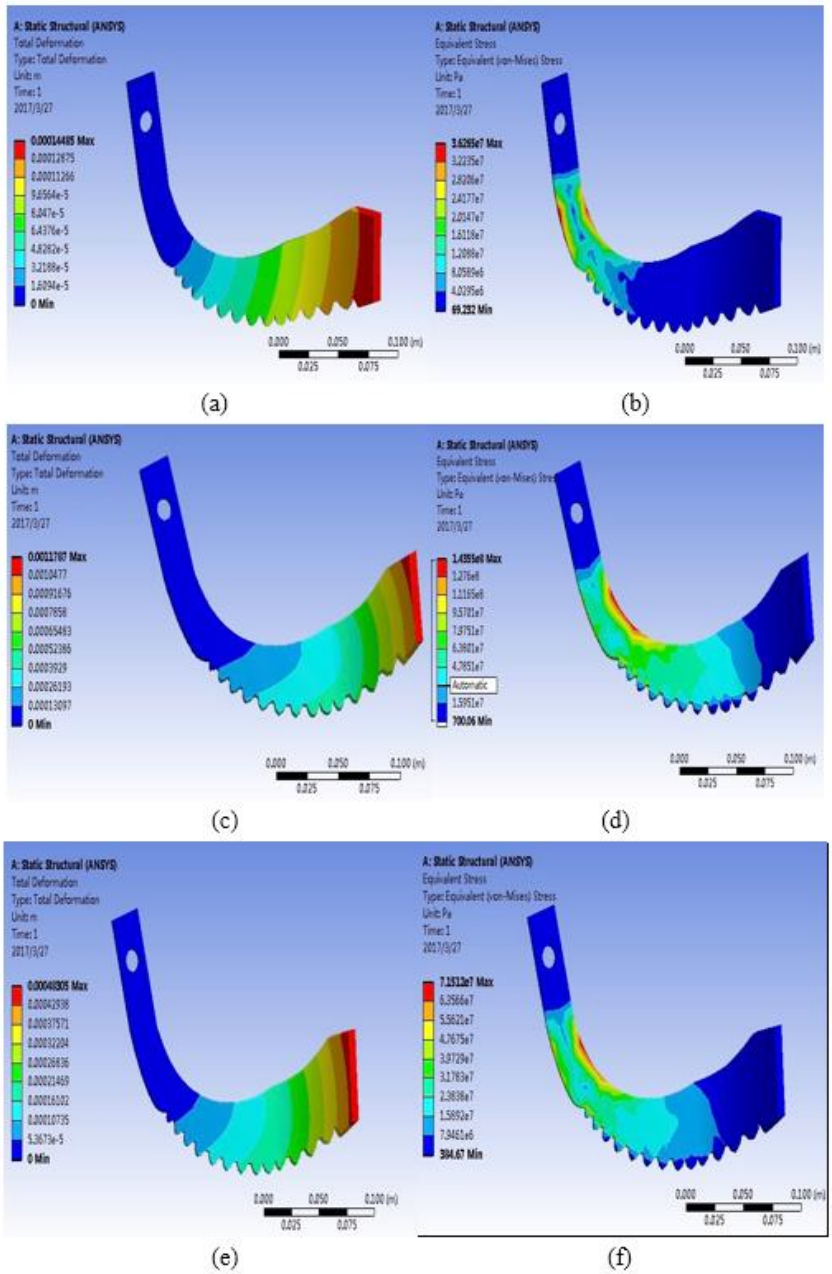

Figure 5. Force analysis diagrams of the bionic rotary blade (a. Total deformation of the loaded bionic rotary blade side edge; b. Total stress of the loaded bionic rotary blade side edge; c. Total deformation of the loaded bionic rotary blade sidelong edge; d. Total stress of the loaded bionic rotary blade sidelong edge; e. Total deformation of the loaded bionic rotary blade full edge; f. Total stress of the loaded bionic rotary blade full edge**)**

As can be seen from Fig.4e and Fig.4f, when load was applied to the full edge, the maximum deformation was 0.671mm, which occurred on the tool tip after the sidelong edge, and then decreased

towards the side edge. The minimum deformation occurred at the handle and part of the side edge. The maximum stress was 90.46Mpa, which occurred on the inner and outer sides of the joint between the handle and the tool face, and then extended outward and decreased gradually.

3.1.2 Statics analysis of the bionic rotary cutting tool

The statics analysis of the bionic rotary blade adopted different meshing methods for the tooth-form blade and the tool face.

The average pressure loaded on the side edge alone is expressed in (5);

$$p = \frac{F}{S} = \frac{500N}{1055.45mm^2} = 0.47Mpa \quad (5)$$

The average pressure loaded on the sidelong edge alone is expressed in (6);

$$p = \frac{F}{S} = \frac{500N}{538.59mm^2} = 0.92Mpa \quad (6)$$

The average pressure loaded on the full edge is expressed in (7);

$$p = \frac{F}{S} = \frac{500N}{1594.04mm^2} = 0.31Mpa \quad (7)$$

As can be seen from Fig.5a and Fig.5b, when load was applied to the full edge, the maximum deformation was 0.145mm, which occurred on the tip of the sidelong edge, and then decreased towards the side edge. The minimum deformation occurred at the handle. The maximum stress was 36.26Mpa, which occurred on the inner and outer sides of the joint between the handle and the tool face, and then extended outward and decreased gradually.

As can be seen from Fig.5c and Fig.5d, when load was applied to the sidelong edge, the maximum deformation was 1.179mm, which occurred on the tool tip after the sidelong edge, and then decreased towards the side edge. The minimum deformation occurred at the handle and part of the side edge. The maximum stress was 14.36Mpa, which occurred on the inner and outer sides of the joint between the handle and the tool face, and then extended outward and decreased gradually.

As can be seen from Fig.5e and Fig.5f, when load was applied to the full edge, the maximum deformation was 0.48mm, which occurred on the tool tip after the sidelong edge, and then decreased towards the side edge. The minimum deformation occurred at the handle and part of the side edge. The maximum stress was 71.51Mpa, which occurred on the inner and outer sides of the joint between the handle and the tool face, and then extended outward and decreased gradually.

3.1.3 Comparison and analysis of the tool indicators

The things that the prototype rotary blade and the bionic rotary blade have in common: the maximum total deformation occurred at the tip of the sidelong edge of the rotary blade, and the minimum deformation occurred at the handle. The maximum stress occurred near the joint between the handle and the blade back and the minimum stress occurred on the sidelong scoop surface and edge. The differences between the prototype rotary blade and the bionic rotary blade are listed in Table 1:

Table 1. Numerical analysis of different conditions

	Side edge		Sidelong edge		Full edge	
	Max. deformation (mm)	Max. stress (Mpa)	Max. deformation (mm)	Max. stress (Mpa)	Max. deformation (mm)	Max. stress (Mpa)
Prototype rotary blade	0.17	52.23	1.81	17.07	0.67	90.46
Bionic rotary blade	0.15	36.26	1.18	14.36	0.48	71.51
Change rate	11.8%	30.6%	34.8%	15.9%	28.3%	19.0%

It can be seen from Table 3-1 that the advantage of the bionic rotary blade is that no matter what kind of force is applied on the cutting tool, the impacts on the stress and deformation of the tool are reduced.

3.2 Soil statics analysis and comparison of rotary tillage

3.2.1 Soil statics analysis of the prototype rotary blade

The soil model was a 500×500×300(mm) cube, and the diagrams were drawn according to the instantaneous position at which the tool cut vertically into the soil (Wang et al., 2006; Che, 2008; Zhang, 2003). The model is shown in Fig.3-3a. Considering the force interactions, we applied a uniform load of 500N onto the soil contact surface:

$$p = \frac{F}{S} = \frac{500N}{571.28mm^2} = 0.88Mpa \quad (8)$$

The analysis results are shown in Fig.6b, 6c and 6d, which cover the analysis of the total stress, total deformation and the strain in the forward direction in the soil model of the prototype rotary blade.

According to Fig.6b, the stress was mainly concentrated in the parts of the tool that contacted the soil, and the stresses in other parts experienced almost no change. According to Fig.6c, the deformation in the soil decreased from the tool to the surroundings, and the displacement ranged between 36.66-64.19mm, with the maximum value being 82.47mm. According to Fig.6d, the maximum soil displacement was -78.58mm, and the soil all shrank towards the centre of the tool.

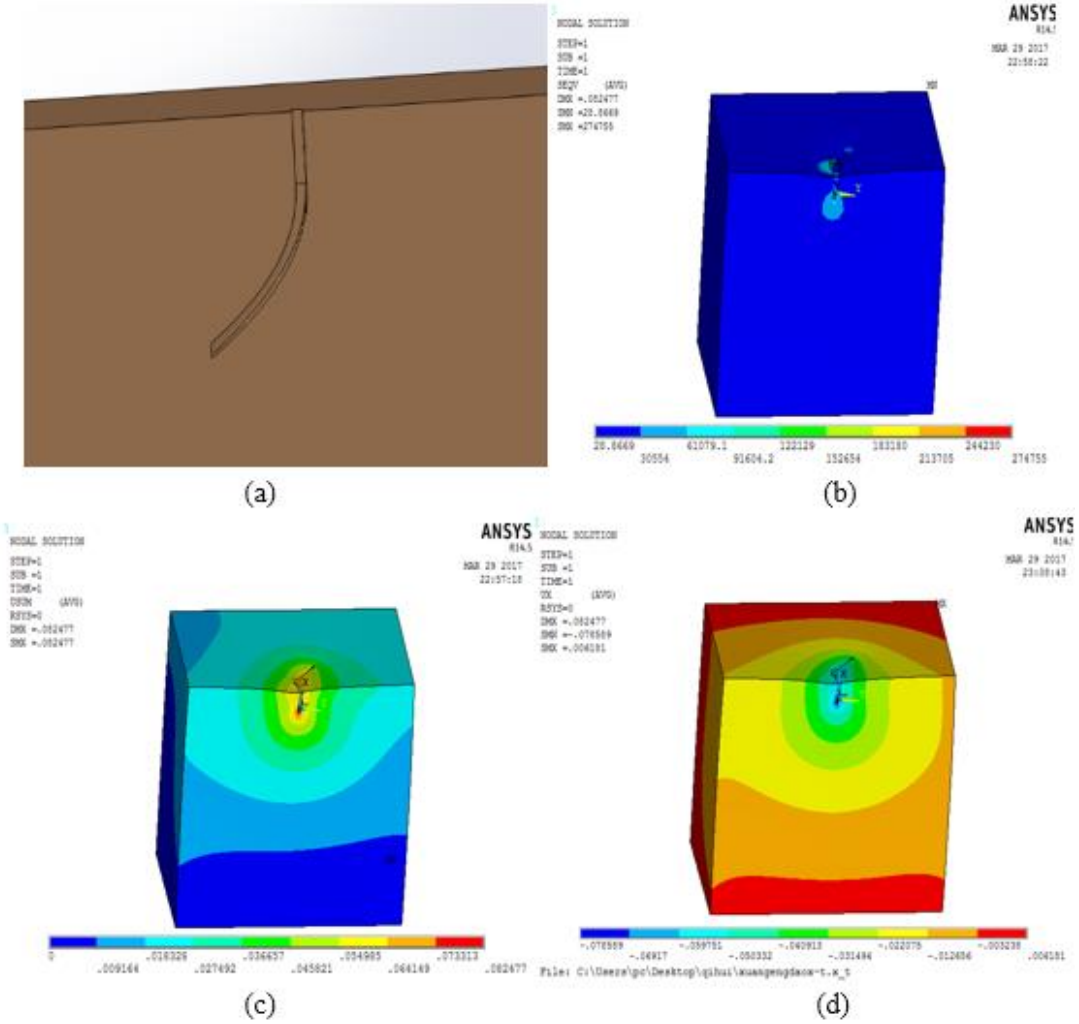

Figure 6. Soil statics analysis diagrams of the prototype rotary blade (a. Soil model for the prototype rotary blade with the maximum tillage depth; b. Diagram of total soil stress for the prototype tool used in rotary tillage; c. Diagram of total soil deformation for the prototype tool used in rotary tillage; d. Diagram of soil deformation in the forward direction for the prototype tool used in rotary tillage**)**

3.2.2 Soil statics analysis of the bionic rotary blade

As shown in Fig.7a: considering the force interactions, we applied a uniform load of 500N onto the soil contact surface:

According to Fig.7b, the stress was mainly concentrated in the parts of the tool that contacted the soil, with the maximum stress being 0.005Mpa, and the stresses in other parts experienced almost no change.

According to Fig.7c, the deformation in the soil decreased from the tool to the surroundings, and the maximum displacement was 0.034mm.

According to Fig.7d, the maximum soil displacement was close to 0.

$$p = \frac{F}{S} = \frac{500N}{757.29mm^2} = 0.66Mpa \quad (9)$$

3.2.3 Comparison and analysis of the soil model indicators

When the bionic rotary blade is cutting into the soil, there was little or even no deformation of soil around the tool. With the aid of the saw teeth, the soil cut out was temporarily stored in the tooth throat and did not cause any soil extrusion. When rotated out of the soil surface, the stored soil would be thrown out to achieve the rotary tillage effect.

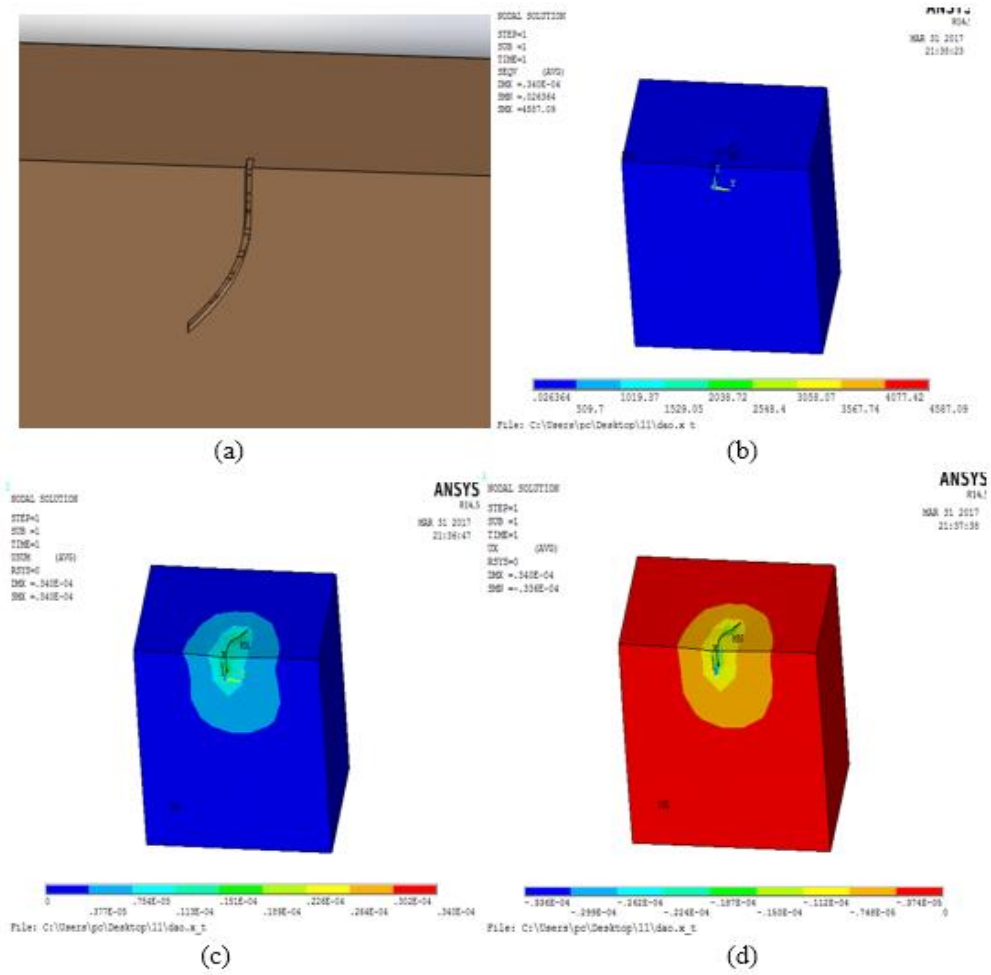

Figure 7. Soil statics analysis diagrams of the bionic rotary blade (a. Soil model for the bionic rotary blade with the maximum tillage depth; b. Diagram of total soil stress for the bionic tool used in rotary tillage; c. Diagram of total soil deformation for the bionic tool used in rotary tillage; d. Diagram of soil deformation in the forward direction for the bionic tool used in rotary tillage**)**

4 FIELD COMPARISON TEST ON THE ROTARY CUTTING TOOLS

The test equipment used are shown in Fig.8a; the agricultural machinery testing ground in Anhui Agricultural University was selected as the testing ground, as shown in Fig.8b. The tillage depth, soil crushing rate and soil flatness after the tool started working were measured according to GB/T 5668.3-1995

Figure 8. Test equipment and testing ground (a. Test equipment; b. Testing ground for agricultural machinery**)**

4.1 Rotary tillage width and stability test

The rotary tillage stubble cleaner was switched to the rotary tillage operation mode, with a knife roll rotational speed of 430r/min, to mainly measure the tillage depth and stability indicators.

Two working conditions were tested. In working condition 1, the average speed is 0.53m/s and in working condition 2, it is 1.02m/s. Under each working condition, three travels were tested. The rotary tillage performance test results of the prototype and bionic rotary blades are listed in Table 2 and 3.

Table 2. Rotary tillage test data of the prototype rotary blade

Rotary tillage performance test results of the prototype rotary blade					
Item		Travel 1	Travel 2	Travel 3	Average
Tillage depth/mm	Working condition 1	118	114	115	116
	Working condition 2	106	105	110	107
Tillage depth stability coefficient %	Working condition 1	93.78	91.89	94.23	93.30
	Working condition 2	95.13	91.06	92.44	92.88
Tillage width/mm	Working condition 1	2302	2296	2278	2292
	Working condition 2	2306	2301	2305	2304
Tillage width stability coefficient %	Working condition 1	98.23	98.54	98.67	98.48
	Working condition 2	98.31	98.54	98.74	98.53

Table 3. Rotary tillage test data of the bionic rotary blade

Rotary tillage performance test results of the bionic rotary blade					
Item		Travel 1	Travel 2	Travel 3	Average
Tillage depth/mm	Working condition 1	120	119	117	119
	Working condition 2	108	106	112	109
Tillage depth stability coefficient %	Working condition 1	93.63	92.14	94.11	93.29
	Working condition 2	94.03	91.41	92.32	92.58
Tillage width/mm	Working condition 1	2303	2298	2284	2292
	Working condition 2	2305	2300	2306	2304
Tillage width stability coefficient %	Working condition 1	98.35	98.51	98.45	98.44
	Working condition 2	98.23	98.61	98.88	98.57

Judged by the testing data, there is no obvious difference between the effects of the prototype rotary blade and the bionic rotary blade in soil tillage depth and width, and almost no impact on the stability.

4.2 Determination of the post-tillage soil crushing rate

The data collected are listed in Table 4:

Table 4. Test data of soil crushing rate

Soil crushing rate % (≤40mm soil block)					
Prototype rotary blade	1	2	3	4	5
	73.84	76.41	71.73	75.41	72.33
Bionic rotary blade	1	2	3	4	5
	74.18	78.93	74.43	76.12	74.58
Average soil crushing rate of the prototype rotary blade: 73.94					
Average soil crushing rate of the bionic rotary blade: 75.64					

As can be seen from Table 4, the bionic rotary blade has some advantage in soil crushing rate over the prototype rotary blade – the soil crushing rates of the former were all greater than the national standard 65%.

4.3 Determination of the post-tillage soil flatness

The measured data of soil flatness are listed in Table 5:

Table 5. Data table for soil surface flatness determination

	Prototype rotary blade (mm)			Bionic rotary blade (mm)		
Measure point	Distance to the measure point	Average	Standard deviation	Distance to the measure point	Average	Standard deviation
1	30			15		
2	36			37		
3	45			0		
4	67			46		
5	57	39	20.15	51	30	14.76
6	48			32		
7	72			24		
8	0			18		
9	28			41		
10	35			32		

According to Table 5, after the bionic rotary blade was used, the soil was quite flat and smooth.

5 CONCLUSIONS

This paper takes the saw teeth on the moving chela of the crab cheliped as the bionic object and designs a kind of bionic rotary cutting tool. It also analyses and tests such tool. And the conclusions are as follows:

(1) This paper performs morphological analysis on the teeth arranged on the moving chela of the crab cheliped, extract their profile curves and obtains their geometrical parameters through fitting. In this way, the optimal curve and analytic equation for the bionic tooth form design are obtained, of which the equation is expressed as follows:

y=(0.03766/(0.11282*sqrt(PI/2)))*exp(-2*((x+0.07006)/0.11282)^2)

(2) The simulation results of the prototype rotary blade and the bionic rotary blade are analysed: both the stress and deformation of the bionic rotary blade are reduced to different extents. The bionic rotary blade focuses on cutting the soil and discharges it to the soil surface through the tooth throat.

(3) The test on the performance of the prototype rotary blade and the bionic rotary blade shows that the latter has more advantages in the rotary tillage operation.

6 REFERENCES

►Chen,Y. J. (2008). Study on Sugarcane - soil System Simulation Model, Guangxi University.

►Ding, W. M., Peng, S. Z. (1995). Research on Grass-removing Angles and Equations of Rotary Blades Affiliation, Transactions of the Chinese Society of Agricultural Engineering, 2, 68-72.

►Duan, Y. H., Xiao, Z. R., Zhang, Z. (2005). Rigid piles. Three - dimensional Finite Element Analysis of Mechanical Behavior of Flexible Pile Composite Foundation, Chinese Journal of Geotechnical Engineering, 8(7), 27-29.

►Ge, Y., Wu, X. F, Wang, L. (2007). Stress Simulation of Rotary Tiller Based on ANSYS Micro Tiller, Journal of Shihezi University, 5(25), 627 -629.

►Gill, W. R. Vanden Berg, G. E. (1967). Soil Dynamics in Tillage and Traction, Agricuture Handbook No.316, United States Department of Agiculture, 1967.

►Gill, W. R.,Vanden Berg, G. E. (1967). Soil dynamics in tillage and traction, Agriculture Handbook. United States Department of Agriculture.

►Lu J. F., Zhang K. K., Zhang F. G. (2015). The optimization design of micro-cultivator blade used on sloping fields, Mathematical Modelling of Engineering Problems, 2(2), 1-4.

►Luo, H. J. (2005). Application of Orign7.0 in Chemical Numerical Calculation, Journal of Anhui University of Science and Technology, 25(1), 67-70.

►Qu, Z. J. (1987). Soil Plasticity Mechanics, Sichuan:Chengdu University of Science and Technology Press.

►Ren, L. Q., Tong, J., Li, J. Q., Chen B. C. (1999). Soil Adhesion and Biomimetics of Soil-engaging Components in Anti-adhesion Against Soil:areview, Proceedings 13th International Conferece ISTVS, Munich Germany, 145-152.

►Ren, L. Q., Yan, B. Z., Cong, Q. (1999). Experimental Study on Bionic Non-smooth Surface Soil Electro-osmosis, International Agriculture Engineering Journal, 8(3), 185-196.

►Tong, J., Ren, L. Q., Chen B. C. (1998). Chemical Constitution and Abrasive wear Behaviorof Pangolin Scales, Journal of Materials Science Letters, 17(6), 523-525.

►Tong, J., Ren, L. Q., Chen, B. C. (1994). Geometrical Morphology Chemical Constitution and Wettability of Body Surfaces of Soil Animals, International Agriculture Engineering Journal, 3(1-2), 59-67.

►Wang, X. J., Zhou, W. Y., Jiang, X. Application of ANSYS in Simulating Pile - soil Contact, Forest Engineering, 22(3), 49-51.

►Zeng, D. C. (1995). Mechanical Soil Dynamics, Beijing: Beijing Science &Technology Press.

►Zhang, S. M. (2003). Structural Analysis Based on Finite Element Software ANSYS7.0, Beijing: Tsinghua University Press.

►Zhu, L. X., Yang, L., Zhu, C. (2014). Finite Element Analysis of The Rotary Tillage Knife Based on ANSYS Workbench, Mechanical Research & Application, 1, 88-89.